Application of Continuous Ramped Heating to Assess Dispersion in Apatite (U-Th)/He Ages: A case study from Transantarctic Mountains of southern Victoria Land

Hongcheng Guo[a,*], Peter K. Zeitler[a], Bruce D. Idleman[a], Annia K. Fayon[b], Paul G. Fitzgerald[c], Kalin T. McDannell[d]

[a] Department of Earth and Environmental Sciences, Lehigh University, Bethlehem, PA 18015
[b] Department of Earth Sciences, University of Minnesota, Minneapolis, MN 55455
[c] Department of Earth and Environmental Sciences, Syracuse University, Syracuse, NY 13244
[d] Department of Earth Sciences, Dartmouth College, Hanover, NH 03755
* Corresponding author: Hongcheng Guo (hog217@lehigh.edu)

Keywords: Apatite; (U-Th)/He; Thermochronology; Age Dispersion; Helium; Diffusion; Transantarctic Mountains

ABSTRACT

Application of apatite (U-Th)/He thermochronology has been hindered by incomplete understanding of single-grain age dispersion often displayed by samples, particularly those from older, slowly cooled settings. To assess the capability of continuous ramped heating (CRH) to explain dispersion, we performed a study on an apatite suite from Cathedral Rocks in the Transantarctic Mountains (TAM) that have high age dispersion. Examining 132 apatite grains from a total of six samples, we confirmed earlier apatite (U-Th)/He results showing that measured AHe ages have at least three-fold intra-sample dispersion with no obvious relationships between ages and effective uranium concentration (eU) or grain size. CRH results on these apatites yielded two groups. Those with younger ages, characterized by single-peak incremental ^{4}He gas-release curves, displayed simple volume diffusion behavior. In contrast, grains with older ages generally show anomalous gas release in the form of sharp spikes and / or extended gas-release at high temperatures (i.e., >= 800 °C). Well-behaved apatites still show considerable age dispersion that exceeds what grain size, radiation damage, and analytical uncertainty can explain, but this dispersion appears to be related to variations in ^{4}He diffusion kinetics. The screened AHe ages from well-behaved younger apatite grains together with kinetic information from these grains suggest that the sampled region experienced slow cooling prior to rapid cooling (rock exhumation) beginning *ca.* 35 Ma. This interpretation is consistent with other studies indicative of an increase in exhumation rates at this time, possibly related to the initiation of glaciation at the Eocene-Oligocene climate transition. An attempt to correct anomalous older apatite ages by simply removing extraneous gas-release components is proposed yielded some ages that are too young for the samples' geologic setting, suggesting that the factors that lead to anomalous laboratory release behavior can impact both the expected radiogenic component as well as those that are extraneous. From our observations we conclude that: (1) CRH analysis can serve as a routine screening tool for AHe dating and offers opportunities to reveal first-order kinetic variations; (2) model-dependent age correction may be possible but would require some

means of estimating the broad proportions of ^{4}He components incorporated into grains before and after closure to diffusion, and (3) interpretation of highly dispersed AHe ages requires assessment of individual-grain diffusion kinetics beyond that predicted by radiation-damage models. We also infer that many apatite grains contain imperfections of varying kinds that contribute significantly to kinetic variability beyond that associated with radiation damage.

1. Introduction

Following the proposal that apatite (U-Th)/He (AHe) ages could be used as a low-temperature thermochronometer (Zeitler, 1987), advances in pursuing the fundamental diffusion systematics and kinetics of helium release (Wolf et al., 1996; Farley et al., 1996; Farley, 2000; Shuster et al., 2006; Flowers et al., 2009) has led apatite (U-Th)/He thermochronology to become widely used in studies of tectonic and surface processes (e.g., Reiners et al., 2003; Ehlers and Reiners, 2005; Fitzgerald et al., 2006; Flowers and Farley, 2012; Toraman et al, 2014; Long et al., 2015). However, it has become widely recognized that interpretation of AHe data is often complicated by intra-sample age variations (commonly referred as “excess age dispersion”) that are beyond typical analytical uncertainties (e.g., Fitzgerald et al, 2006; Flowers and Kelley, 2011; Peyton et al. 2012; Zeitler et al. 2017; McDannell et al. 2018). Significant efforts have been made to explain such age dispersion and to unravel complexities in ^{4}He diffusion systematics. Some factors, for example the presence of U-rich micro-inclusions (Farley, 2002), U and Th zonation (Meesters and Dunai, 2002, Fitzgerald et al., 2006), and ^{4}He implantation (Spiegel et al., 2009, Murray et al., 2014) will complicate He analysis or diffusion systematics in ways that make it difficult to obtain useful apparent ages (Farley, 2000). Other effects such as grain size (Reiners and Farley, 2001), broken grains, (Beucher et al., 2013; Brown et al., 2013) and the way that radiation damage systematically alters He diffusion kinetics (Shuster et al., 2006; Gautheron et al., 2009; Flowers et al, 2009; Willett

et al., 2017) can lead to age dispersion that can be exploited to reveal more information about thermal history. Slow cooling through or long-term residence within an apatite (U-Th)/He partial retention zone will accentuate age dispersion, often to a considerable degree (e.g., Reiners and Farley 2001; Fitzgerald et al., 2006).

Despite these contributions, there are still situations where we still cannot fully explain commonly observed AHe age dispersion. Applied studies of sample suites from different geologic settings have found that even using careful sample selection, grain size and radiation damage can only explain some of the observed dispersion (Zeitler et al., 2017). To reduce the probability of overdispersed ages and to understand age dispersion should this occur, common practices include performing “re-extracts” to evaluate if all He has been out-gassed, collecting data only from single-grains, performing large-n replicate analyses, and plotting He ages vs. size (radius) and effective uranium [eU] to evaluate excess dispersion. If excess dispersion occurs, complex data sets can be vexing and difficult to interpret and use in thermal history modeling, and if a large number of samples and single-grain analyses are undertaken in order to circumvent such issues, these approaches are time-consuming and costly.

As a result, the thermochronology community is actively working on the challenge that excess age dispersion presents (e.g., Zeitler et al., 2017; McDannell et al. 2018). A possible factor in age dispersion that has attracted recent attention is the role that crystal imperfections of various types can play in changing diffusion behavior (Djimbi et al., 2015; Fayon and Hansen, 2015; Gerin et al., 2017; Zeitler et al., 2017), adding to the impact that imperfections associated with radiation damage have on diffusion kinetics. This focus

is not a new concept, as Farley (2000) argued that *"Regardless of model, a critical question for apatite helium thermochronometry is whether the total abundance of defects affects the helium retentivity in the low temperature regime and, if so, how and when the defects are acquired."*

Here, we use a recently developed analytical approach, continuous ramped heating (hereafter, CRH, Idleman et al., 2018) which is described in **section 2.2**, to assess this long-standing problem of excess AHe age dispersion by closely examining samples from a well-characterized geological setting. In a broad survey of natural samples, McDannell et al. (2018) suggested that CRH should be able to identify variable ^{4}He outgassing behavior in the form of differing gas-release components. Our work aims to test this suggestion using a classic sample suite (Fitzgerald et al., 2006) from the Ferrar Glacier area of southern Victoria Land in Transantarctic Mountains that yielded highly dispersed AHe ages (section 2.1). We seek to better document how CRH can reveal relationships between AHe ages and ^{4}He outgassing behavior such that it can be deployed as a routine sample-characterization tool to extract interpretable data from complex sample sets.

2. Study Material and Analytical Methods

2.1. The Transantarctic Mountain apatite suite

Ideal apatite samples for our study should (1) have significant dispersed AHe ages, which is not uncommon, but also (2) carry other thermochronologically and geologically constrained thermal history (i.e., rock cooling history; local or regional geological events) to allow assessment and interpretation of dispersed data, which is challenging. The Transantarctic Mountains are a good locality to test our questions because their tectonic

and thermochronological setting is well established and their overall history of slow cooling since the Mesozoic will tend to amplify any dispersion in AHe ages which may be due to variations in ^{4}He diffusion systematics. We have selected a vertical profile collected from basement granitoids in the Ferrar Glacier area of southern Victoria Land in the Transantarctic Mountains – Cathedral Rocks – because of its thermal history, as well as the availability of both AHe and apatite fission track (hereafter, AFT) age constraints from previous studies (e.g., Fitzgerald et al. 1992; 2002). Those studies suggest the locality also experienced relatively rapid cooling early in the Oligocene, possibly resulting from the onset of glacial incision or a change in tectonics.

The Transantarctic Mountains (**Fig. 1)** have long been regarded as an intriguing feature owing to their large size (>2500 km long), high elevations (>4 km) and the way they define the western flank of the West Antarctic rift system, in essence separating the significantly different geological terranes of East and West Antarctica (e.g., Dalziel 1992, Fitzgerald, 2002, Goodge 2020). The West Antarctic rift system underwent two phases of extension, early initiation in the middle Mesozoic (e.g., Elliot and Fleming, 2004), and then a later post-Eocene phase (e.g., Wilson et al., 1998; Florindo et al., 2001; Smellie, 2001). In many locations along the TAM including the Ferrar Glacier region, the mountains have a layer-cake stratigraphy that dips (1-2°) gently inland before disappearing under the East Antarctica Ice Sheet (e.g., Gunn and Warren 1962; Goodge 2002). In southern Victoria Land basement rock is dominated by the arc-related Cambro-Ordovician magmatic suite of the Granite Harbour Intrusives (e.g., Allibone et al. 1993) intruded into polydeformed metasedimentary rocks (e.g., Goodge 2020) during the Ross Orogeny. Devonian to Triassic flat-lying sedimentary rocks known as the Beacon Supergroup were then

deposited unconformably on a basement erosion surface. Basin sedimentation was subsequently ended by extensive basaltic flood magmatism marking the breakup of Gondwana, expressed in southern Victoria Land as the Ferrar Dolerite, presenting as thick (~300 m) sills within basement, and along the unconformity, as well as thinner sills distributed within Beacon sediments (e.g., Gunn and Warren 1962). Subsequent to Ferrar magmatism, the TAM was formed largely related to uplift along the West Antarctic rift flank (e.g., Fitzgerald 1992).

There is a rich collection of thermochronology studies in southern Victoria Land, both onshore (Gleadow et al., 1984; Gleadow and Fitzgerald, 1987; Fitzgerald and Gleadow, 1988; Fitzgerald 1992, 2002; Olivetti et al., 2018) and offshore (Fitzgerald 2001, Olivetti et al., 2013) that generally indicate episodic exhumation with periods of enhanced cooling and exhumation (though slow relative to most active orogens) in the Cretaceous and Cenozoic. Fitzgerald et al. (2006) sought to explore the younger part (less than ca. 50 Ma) of the exhumation history by integrating AFT data with inverse thermal models, combined with, what at that time, was the relatively new approach of apatite (U-Th)/He dating. However, apatite (U-Th)/He ages from two vertical profiles collected on either side of the Ferrar Glacier displayed considerable single-grain age variation (**Fig. 1)**. Thus, the focus of that study shifted from constraining the younger exhumation history of the TAM towards documenting and exploring why over-dispersion occurs and how such data might be interpreted. Nevertheless, constraints on the cooling and exhumation history of this part of the TAM were obtained. With less AHe age dispersion within data from the north side vertical profile (Peak 1880) the interpretation was more complete: slow cooling (exhumation) from Late Cretaceous to early Eocene (~1°C/Myr), an increase at ca. 43

Ma, slowing again until an increase in the late Eocene (ca 37–35 Ma). On the south side of the glacier AHe data from a vertical profile from the eastern-most of the peaks of the Cathedral Rocks had much greater age dispersion that the Peak 1880 profile, thus the interpretation relied mainly on AFT data/models and the AHe ages added very little to our understanding of the younger cooling history. At Cathedral Rocks, the interpretation was that cooling/exhumation was relatively slow (~1°C/Myr) from Cretaceous to the early Cenozoic with slightly faster cooling/exhumation beginning ca. 50 Ma (~2.8 °C/Myr).

For CRH screening and AHe dating, apatite grains were selected from six samples from the Ferrar Glacier profile at Cathedral Rocks, originally labeled R22641, R22642, R22643, R22644, R22645, R22646 from high to low elevation (Fitzgerald et al., 2006). To simplify communication, we renamed them R1, R2, R3, R4, R5, R6, respectively, in the following discussion. All apatite grains were picked, examined, and photographed using a Nikon SMZ800 microscope under plain light at ~95 × magnification for optical characterization to determine shape and size for calculation of alpha-ejection correction factors and to assess basic grain characteristics such as presences of crystal imperfections such as inclusions, euhedral-vs-anhedral shape, and grain integrity (see **Research Data – Table A1**).

2.2 Sample Characterization

2.2.1 Chemistry

To document their overall composition as well as variability, we analyzed a number of grains from two samples (R1 and R2) by electron microprobe. Complete results are found in the online archive; Table 1 summarizes results by averaging data for all spots for all

grains. Only Si, Ce, and F show some modest scatter, but Si and Ce are present at low concentrations. The grains are all fluorapatite in composition, with an average proportion for Fap:Cap:Hap (Piccoli and Candela, 2002) of 0.859 : 0.007 : 0.133 . Values of the fission-track annealing parameter *rmr0* (Ketcham et al., 2007) calculated from the elemental analyses range from 0.829 to 0.840, signifying near endmember fluorapatite (**Appendix A – Fig. A.1**).

	TAMR1	**N=48 spots, 30 grains**			**TAMR2**	**N=51 spots, 30 grains**		
	Mean	**SD**	**CDL99**	**MSWD**	**Mean**	**SD**	**CDL99**	**MSWD**
Si	0.126	0.051	0.006	188	0.150	0.056	0.010	200
Y	0.121	0.053	0.030	7.2	0.151	0.057	0.030	8.4
La	*0.044*	*0.031*	0.031	4.3	*0.035*	*0.028*	*0.030*	3.6
Ce	0.195	0.060	0.029	15.4	0.204	0.071	0.030	22.1
Mg	*0.003*	*0.003*	0.006	1.0	*0.008*	*0.015*	*0.010*	1.7
Ca	39.63	0.159	0.010	3.7	39.47	0.222	0.010	9.3
Sr	*0.014*	*0.007*	0.013	1.1	*0.014*	*0.008*	*0.010*	1.6
Na	*0.010*	*0.007*	0.009	2.2	*0.012*	*0.009*	*0.010*	2.2
P	18.53	0.139	0.014	2.0	18.44	0.125	0.010	1.8
S	*0.001*	*0.002*	0.006	0.8	*0.001*	*0.003*	*0.010*	1.0
Cl	0.059	0.027	0.009	13.0	0.043	0.023	0.010	3.3
F	3.179	0.203	0.032	54.0	3.290	0.197	0.030	48.0
O	38.62	0.15			38.44	0.16		
TOTAL	100.53	0.36			100.25	0.42		

Table 1. Electron microprobe analyses of apatites from two TAM samples. Means, standard deviations, and detection limits are in weight percent. MSWD (mean square of weighted deviates) serves as measure of scatter of values relative to instrument uncertainties. Values in italics are near or below detection limit.

2.2.2 Survey of crystallographic defects

We examined polished sections of grains from samples R1 and R2 to assess the prevalence of defects in TAM apatites. Before polishing, grains were annealed at 500 ˚C for 60 minutes to remove any fission tracks, and then etched using two different solutions,

194 a typical 5M HNO_3 solution commonly used for fission-track etching, and also a 0.5 M
195 HNO_3 solution to focus on smaller more delicate structures. Detailed from this work are
196 part of an ongoing study, but for this paper the key observation is that TAM apatite grains
197 are highly variable in defect density, ranging from nearly imperfection-free to being riddled
198 with imperfections of various types (**Fig. 2**).

199 **2.3 Data collection and analysis**

200 Individual grains were placed in closed niobium tubes, degassed of their ^4He via the CRH
201 method at the Lehigh University noble-gas geochronology lab (see below and **Appendix**
202 **B** for details), and measured for parent U-Th-Sm isotopes via dissolution and isotope
203 dilution at the Arizona Radiogenic Dating Laboratory with detailed procedures reported
204 by Reiners and Nicolescu (2006).

205 **2.3.1 Continuous ramped heating**

206 The CRH method characterizes the diffusive loss of ^4He by continuous heating following
207 a progressively increasing temperature schedule, typically at a fixed rate. Evolved He is
208 measured continuously as a function of time and temperature (Idleman et al., 2018). Our
209 early experiments (Idleman et al., 2018; McDannell et al., 2018) used a resistance furnace
210 for heating, which we have now replaced with a fiber-coupled diode laser system. The
211 laser provides more precise time and temperature control, less temperature lag (i.e.,
212 better response time), and lower loads of potentially interfering active gases coevolved
213 with He. Here we briefly outline the most recent analytical procedure of our
214 implementation of CRH and include a complete documentation of this CRH procedure in
215 **Appendix B**. We also provide our observations made on the behavior of standard

Durango apatite to document the behavior of simple ^{4}He diffusion systematics as measured by our newest application of the CRH method.

2.3.2 Sample handling

After being selected and photographed, each apatite grain was placed in a closed clean niobium (Nb) tube, which had been cleaned and degassed for 3 hours in a vacuum furnace at 600 °C. The tube was then placed in a hand-made Nb foil envelope ~4 mm in diameter that had also been prewashed and degassed. We used these small envelopes to present an even, flat surface to the laser beam in order to achieve better temperature control and measurement. The packages were placed in quartz-glass holders located in a mobile sample rack that allows us to load multiple samples and analyze them without breaking vacuum.

2.3.3 Data collection

Each CRH run was performed under static vacuum conditions with the mass spectrometer directly open to the sample cell. At the beginning of an analysis, the extraction line was isolated from its pumping system and the ^{4}He beam was measured and recorded for 3 – 4 minutes, allowing us to estimate cold-blank accumulation rates before the initiation of heating. After heating began, temperatures were recorded by an optical pyrometer capable of measurement over a range of ~180 to >1200°C. Peaks at masses 1, 2, 3, 4, and 28 were measured and recorded continuously using a Balzer Prisma Plus quadrupole mass spectrometer. Besides ^{4}He, the peaks corresponding to H, H_2, HD, and N_2 were monitored because we have found that in some runs at high levels these active gases can have a moderate impact on ^{4}He sensitivity by attenuating the

mass 4 beam at temperatures greater than 850 to 900 °C. Two SAES GP50 getter pumps (operated at 20°C and 200°C) were used to reduce the partial pressures of these active gases during analysis so that their effects on ^{4}He were never more than a few percent at high temperatures, when hydrogen and nitrogen attain their highest levels (up to 100x those at seen in the cold background signal).

All samples were heated to a temperature of at least 800°C. Samples that continued to outgas ^{4}He at 800°C were heated further until they showed no additional ^{4}He contribution for at least 1 minute, or until they reached 1100°C (whichever came first). After allowing 2-3 minutes for sample cool-down and additional purification of the evolved ^{4}He, a metered aliquot of about ^{4}He of 2.22×10^{-13} mol was introduced to allow determination of the total ^{4}He by the method of standard additions. In some cases, this post-run cleanup step was preceded by a small increase in the total-release ^{4}He signal (rarely exceeding 5%), reflecting gettering of the active gas species suppressing ^{4}He sensitivity. This small suppression does not have a significant impact on relative patterns of CRH release behavior but is clearly important to eliminate before measuring the final ^{4}He abundance for accurate age determination.

2.3.4 Data reduction

During our CRH runs for the Cathedral Rocks apatites, individual crystals were heated at a fixed rate of 30°C/minute, and temperature and ^{4}He measurements were recorded every 10 seconds. To smooth noise in the measured sample temperatures, particularly at low temperatures, we performed a rolling 11-point linear regression of the measured temperatures and registered the times of ^{4}He measurement blocks with the regressed

temperature record through interpolation. In practice, sample temperatures determined in this way agree with the targeted setpoint temperatures defined by the heating schedule to within 2-3°C. The ^{4}He beam values were then corrected for dynamic background and evolved blank, yielding final CRH results in the form of tables of time, temperature, and corrected ^{4}He beam values. From these results we calculated the first derivative of fractional loss (*f*) to construct incremental ^{4}He loss curves (*df/dT vs T,* hereafter *df* as shorthand) and extract kinetic data (ln (D/a_2), (1/s), and *10000/T* (K)) for each sample. These data are available in the data repository as **Table A2** and **Table A3**.

2.3.5 Expected behavior: Durango apatite

We carried out CRH analyses of Durango apatite, an apatite standard widely used by the thermochronology community known for its reproducibility in AHe age (McDowell et al., 2005) and ^{4}He diffusion kinetics (Farley, 2000) with two goals: using its degassing behavior as a benchmark for expected CRH gas-release patterns and using its kinetics to test analytical reproducibility. We performed CRH screening on both internal fragments and abraded balls that were made from air abrasion experiments using an apparatus similar to that described by Krogh (1982).

The spherical-equivalent radii (Ketcham et al., 2011) of our grains ranged from 99 to 118 μm for the shards and from 90 to 167 μm for the balls. In general, *df* curves for both the shards and balls (**Fig. 3A**) exhibit the simple, consistent unimodal peaks predicted by volume diffusion theory (see modeled ^{4}He outgassing behavior via volume diffusion under CRH in Idleman et al., 2018 and McDannell et al., 2018). We intentionally include results from balls with varying radius to show the precision of our CRH temperature control. With

282 the same heating schedule of 30°C/min, the larger grains show a slightly higher-
283 temperature peak-gas release (McDannell et al., 2018) compared to medium-sized balls
284 (**Fig. 3A**), and the peak-gas release occurred at lower temperatures for one of the
285 smallest balls despite some moderate roughness.

286 This size-controlled kinetic variability is also evident on the Arrhenius plot (**Fig. 3B**) where
287 these grains overall show similar behavior but with offsets from published kinetics by
288 different extents that generally reflect their sizes. After recasting all the results to the same
289 radius (80 μm, **Fig. 3C**), we effectively removed the effect of grain size. Because the
290 estimated spherical-equivalent radii of the balls are far more accurate and consistent than
291 that of the shards, we use the remaining kinetics variation within these balls as an
292 estimate of temperature uncertainty. At observed values of ln (D/a^2) of -14 and -12 1/s,
293 the measured temperature ranges for the size-corrected data are 310.5 ± 8.0 °C and
294 375.1 ± 7.8 °C, respectively, consistent with the variation we observe when we perform
295 calibration of the optical pyrometer against a reference thermocouple.

296 **2.3 Technical issues**

297 Using affordable hardware, a single CRH analysis can be done quickly in about the same
298 time as a conventional He analysis, and so represents a potentially routine screening tool
299 that every thermochronology laboratory can perform. There are a few technical issues
300 that are important to appreciate in order to fully understanding the data from this study.
301 These technical concerns have implications for measurement of low-temperature kinetics
302 (**Fig. 3B, C; Fig. 8**) and for overall data precision.

The major challenge when undertaking CRH experiments is temperature measurement, especially in the low-temperature regime (i.e., < 250°C). To increase sample throughput, we measure temperature for each grain using an optical pyrometer rather than a thermocouple. The pyrometer is calibrated with a thermocouple-instrumented sample packet each day before CRH runs. However, two difficulties prevented us from obtaining a robust temperature measurement below ~300°C. First, at the time of sample analysis, our pyrometer had a lower temperature limit of ~198°C. Second, due to the time needed for a sample package to reach thermal equilibrium at low temperatures we often observed (1) temperatures recorded from the pyrometer that were lower than that from the reference thermocouple right after laser startup until ~300 °C and (2) spikes of higher-than-expected temperature readings (laser overshooting) during this time period. The net apparent effect seems mostly to be lower-than-expected ^{4}He release at low temperatures that created significant non-linear trends in Arrhenius plots of Durango apatites (**Fig. 3B, C**), which have been shown to give linear trends during long heating experiments at low temperatures (Farley, 2000). We call out this issue because even after later changes to laser software and new hardware (pyrometer) we found the problem remains, though it is much improved, and so we caution against using our current CRH data for fully quantitative measurement of Arrhenius parameters at low temperatures. Note that this is not a significant problem because in natural samples that are not from internal shards, both alpha-ejection and diffusion profiles will lead to concave-upward Arrhenius trends at low temperatures, ruling out use of these data for kinetic quantification in any case.

3. Results from TAM apatite samples

We analyzed 132 single apatite grains from six rocks collected from the Cathedral Rocks vertical profile (Fitzgerald et al., 2006). For each apatite grain, we obtained its CRH ^{4}He-outgassing curve, AHe age, corrected AHe age (see section 3.4), and ^{4}He diffusion kinetics. We also use thermal histories constrained by Fitzgerald et al. (2006) from AFT data to predict AHe ages using the RDAAM model, allowing us to explore any age dispersion remaining after removing effects of varying radiation damage and grain size. These direct results are presented in this section, and raw data for the CRH runs and U-Th-Sm measurements are included in the data repository (**Table A1, A2, A3**).

3.1. AHe total-gas ages and ^{4}He-outgassing behaviors

For each of the six rock samples, at least 20 grains were analyzed by CRH, and the single-grain total-gas ages were found to be highly dispersed (**Fig. 4; Fig. 5; Data Repository – Table A1**). The intra-sample age dispersion is not surprising, given what we have seen in the ages acquired by Fitzgerald et al. (2006) and the larger size of our data set. Except for a few old outliers that range up to 456 ± 13 Ma, and one young outlier of 6.7 ± 0.2 Ma, these apatites have ages ranging from 27.7 ± 0.9 to 165 ± 7 Ma (see **Data Repository – Table A1**). We observed ^{4}He -outgassing curves (*df*) whose shapes were nearly identical to what volume diffusion theory predicts, as well as some that were anomalous compared to theoretical behavior. Anomalous ^{4}He-outgassing curves were characterized by sharp gas-release spike(s), delayed gas-release at high temperatures, or frequently a combination of both. To assist description and discussion we call apatite grains having *df* curves characterized by smooth unimodal peaks as giving “expected” results (i.e., they passed CRH screening), and samples showing gas spikes and high-temperature release as giving “anomalous” results that failed CRH analysis.

All the analyzed apatites either show one or two gas-release peaks, where the early peak always occurred in the range 572 ± 45°C (uncorrected for grain size). Less than half of the apatite grains survived CRH screening for each of the six samples, and these apatites have greater consistency in gas release, with the peak occurring at 590 ± 35 °C except for a few exceptions whose *df* curves were either broader or narrower than normal and/or whose peak gas-release occurred at temperature ~50 to 100 °C from the aforementioned common range (**Fig. 6; Appendix A – Fig. A.2**). The apatites that survived CRH screening lost at least 90% of their total ^{4}He between ~300 and 750°C, and their He ages are generally younger, ranging from 30.6 ± 1.3 to 56.7 ± 1.0 Ma. The apatites that failed CRH analysis show moderately or significantly anomalous ^{4}He -outgassing behavior, with ages ranging from 33.4 ± 1.0 to >100 Ma. We also found that for each of the six samples, up to seven grains that failed CRH analysis have AHe ages that are older than the AFT central ages reported by Fitzgerald et al. (2006).

3.2. Effects of radiation damage and grain size

All of our AHe total-gas ages should be influenced by variations in radiation damage and grain size to some extent. Our TAM apatite suite has a broad range from ~25 to 100 ppm in effective uranium (hereafter eU; [eU] = 0.238Th + 0.0012Sm; Cooperdock et al. (2019)), and F_T spherical-equivalent radii from ~30 to 75 μm. As in the earlier AHe single-grain dataset from Cathedral Rocks (Fitzgerald et al., 2006), we found no obvious relationship between measured total-gas AHe age and eU or grain size for the entire sample suite (**Fig. 7C, D**). However, moderately strong age-eU and age-size relationships are evident in the subset of apatites that passed CRH screening (**Fig. 7A, B**).

We performed forward modeling by using the thermal histories deduced from AFT data (Fitzgerald et al., 2006), F_T-equivalent spherical radius, and measured eU as input for the HeFTy software (Ketcham, 2005) to predict apparent ages for all of our analyzed apatites by the RDAAM. We then normalized our total-gas ages to these RDAAM ages, calling the resulting ratio the RDAAM-normalization (hereafter, RDN) – samples with values of 1.0 would have ages predicted from their eU, radius, and reference thermal history. For each of the six samples, RDNs are still significantly dispersed (**Fig. 4B; Data Repository – Table A1**) with RDN ages ranging from ~ 0.5 to 3. However, the apatites that survived CRH screening show a narrower range of RDN (typically ~0.5 to 1.5), and these ranges are even narrower if one looks only at RDN from the same individual samples, such as R1, R2, and R6.

3.3. Kinetic variations

Like conventional step-heating analysis, data from CRH analysis allow for the derivation of kinetic information. Using spherical geometry, cumulative fractional loss, the time interval between measurements, and the average sample temperature over this interval, we obtained kinetics data for ^{4}He diffusion for each grain.

We do not intend to use CRH-derived data, at least currently, for precise determination of activation energy, diffusion coefficient, or closure temperature. Rather, we only explore first-order intra-sample kinetic variations evident in the data. This is because: (1) compared to step-heating, CRH's advantage in rapid measurement is offset at very low experimental temperatures by imprecision in measurement of small gas losses, and (2) temperature measurements by optical pyrometry are subject to significant systematic

offsets below ~300°C Despite our hesitation about extracting kinetic parameters from the lowest-temperature portions of the Arrhenius curves, the overall locations of these curves in Arrhenius space are sufficiently well defined and precise (see section 2.2.5) to allow for meaningful comparisons.

We present only the kinetics of those apatites that passed CRH screening (**Fig. 8**), and complete Arrhenius plots for all samples are supplied in Appendix A (**Fig. A.3**). We do this for two reasons: First, we particularly want to explore intra-sample kinetic variations between different well-behaved apatite grains. Second, owing to the fact that kinetic parameters obtained from both step-heating and CRH are sensitive to fractional loss of gas, any presence of gas spike(s), which mostly occurs at low to intermediate temperatures, or a second high-temperature release component breaks the linearity and in fact the justification for Arrhenius relationships.

We obtained a wide range of ^{4}He diffusion kinetics (**Fig. 8A**) for grains giving expected results, and there is a broad correlation between their ages (total-gas age or RDN age) and ^{4}He retentivity, as assessed by relative location on the Arrhenius plot after normalizing for the effect of grain size (**Fig. 8B**) or normalizing for the collective effect of grain size and eU (**Fig. 8C**). Among six samples (**Fig. 8C**), R1 and R2 show a clear correlation between apparent ^{4}He retentivity and either total-gas age or RDN. Sample R6 also shows such a correlation although it does not show very much intra-sample dispersion in total-gas or RDN. Kinetic data from the R6 grains show more subtle variations and less spread on the Arrhenius plot relative to other samples, with the exception of sample R3. Sample R3 did not show any significant intra-sample variation in

^{4}He diffusion kinetics, while variations in both its total-gas age and RDN are significant. Such correlation between age and kinetics is weaker in sample R4 and R5, unless the oldest age in R4 (array of red points) and the youngest age in R5 (array of blue points) are not included.

3.4. Age correction

We attempted to correct the ages of those apatites characterized by anomalous outgassing behavior following the peak-fitting process proposed by McDannell et al. (2018). Based on their assumption that gases released as spikes and at high temperatures are anomalous with respect to the closure process, we started by making synthetic *df* curves using established Durango kinetics and spherical geometry in order to fit the first gas-release peak (i.e., low- to mid-temperature release of gas components). This effectively removes gas spikes and/or delayed gas release at high temperatures (i.e., the second wave of gas release). We used the first peak because (1) the first peak is almost always located at or close to the temperatures at which Durango's peak gas release occurs, (2) the second peak, if present, often appears at temperatures at or above those at which grains controlled by Durango kinetics have lost nearly all of their ^{4}He, and (3) the second peaks occurred over a wide temperature range and often had broad and complex shapes. We discuss the possible complexity of the delayed gas-release further in **section 4**.

Corrected ages were calculated by stripping "extraneous" ^{4}He from the sample release using the synthetic *df* curves as a guide, and then applying the measured U-Th-Sm. Obviously, the ^{4}He correction will always lower ages because the correction process only

436 removes gas component(s). We found that the corrected ages of this apatite suite are
437 much younger than their total-gas counterparts, with most of them correcting to younger
438 than ca. 61 Ma, resulting in a much-reduced intra-sample dispersion (**Fig. 4; Fig. 5**).
439 However, we also noted that, for each sample, some of the corrected ages are as young
440 as ~20 Ma. This is considerably younger than the youngest ages obtained from grains
441 that passed CRH screening or other studies from the area and is probably not plausible
442 geologically (see below).

443 **4. Discussion**

444 Our results on these TAM apatites from Cathedral Rocks vertical profile revealed
445 significant intra-sample dispersion in AHe ages, and the dispersion remains even after
446 accounting for effects of grain size and eU. We found that the dispersion was significantly
447 reduced by CRH screening, and that the screened ages broadly correlate with kinetics.
448 Can these observations be reconciled by a single conceptual model? Below we relate
449 age dispersion to various types of crystal imperfections, followed by discussion of gas
450 components, complexities in age correction, and a proposed conceptual model for 4He
451 retention.

452 **4.1 Radiation damage: only one type of crystal imperfection**

453 Radiation damage, from alpha decay of U and Th, introduces imperfections in apatite
454 grains that act to slow He diffusion (e.g., Gautheron et al., 2009; Flowers et al., 2009).
455 Our results suggest that the dispersion observed in the Cathedral Rocks suite cannot be
456 explained sorely by radiation damage, and therefore require the presence of a broader
457 range of crystal imperfections that add to radiation damage's role in complicating He

diffusion. This interpretation stems from the observation that while samples showing expected diffusion behavior do exhibit possible correlations of age with grain size and eU, they also show broad correlations between age and kinetic parameters. Crystallographic study also suggests that etched apatite grains from this sample suite reveal the presence of dislocations and sub-grain boundaries that can potentially alter kinetic parameters (**Fig. 2**).

4.2 Crystal imperfections terminology

To clarify our discussion, we first define some important terms that have had various usage in the (U-Th)/He literature. First, as used by Farley (2000), the term “defects” or “damage” refers to a broad range of crystal imperfections stemming from thermal and mechanical damage that alters the kinetics of ^{4}He diffusion. In U-Th/He literature the term “damage” has been implicitly used as an equivalence for “radiation damage” because of the development and wide application of the RDAAM model. In order to avoid miscommunication, we will use “crystal defects” as an overarching term to refer to fine-scale imperfections and damage resulting from deformation – dislocations, sub-grain boundaries, grain boundaries and point defects (Karato, 2008), as well as radiation damage; some of these defects (i.e., radiation damage) have been shown to impede diffusion and have been also termed “traps”. Here we prefer to use the term “sink” to refer to a broader range of probably larger imperfections such as fluid inclusions and micro-voids that might act as reversible sinks for diffusing He atoms. Owing to the fact that the term “trap” can depict both objects and processes, in this document we only use “trap” as a verb to describe processes that temporarily “store” He atoms in reversible sinks and separately use “radiation damage” when this kind of diffusion inhibition by defects is

mentioned. To summarize, in our usage and discussion defects are finer-scale imperfections that during the diffusion random walk slow down diffusing He atoms while "sinks" are larger imperfections that can physically trap He atoms and are possibly reversible.

4.3 Outgassing components

Probably the most obvious feature of gas release from an apatite grain that fails CRH screening is the delayed release of ^{4}He at anomalously high temperatures (above ~700 ˚C at a heating rate of 30˚C/min for typical grain sizes), which often represents a considerable amount of gas and produces a second simple unimodal-like gas-release peak on its *df* plot. This component of gas release might result from any types of crystal imperfections that can act as diffusion sinks, such as fluid inclusions (Baxter, 2003), pores (Lippolt et al., 1994; Watson and Cherniak, 2003; Domingos et al., 2020), and microvoids (Zeitler et al., 2017). These features might trap diffusing ^{4}He only temporarily, in proportion to the degree that these sinks are reversible. Given the low solubility of He in apatite (on order 2 x 10^{-11} mol/g-bar; Zeitler et al., 2017), it would seem difficult for any trapped He to re-enter the lattice by solution alone since the changes in pressure that would accompany laboratory heating (2-3x) would be small compared to solubility estimated by Henry's-Law. It thus seems likely that an additional temperature-sensitive mechanism is required to get ^{4}He in sinks to return to the volume-diffusion regime in the lattice.

Another common feature of the He release from apatites that have failed CRH screening is sharp spikes of gas release at low to intermediate temperatures. These spikes can at

503 times account for a considerable amount of the total ^{4}He release, though generally being
504 smaller compared to the ^{4}He released at anomalously high temperatures. These
505 characteristics suggest the presence of very near-surface crystal imperfections which can
506 rupture during heating.

507 **4.4 Evaluation of age correction**

508 Two factors make us question the age-correction procedure as we applied it. First, we
509 noted that age correction does not greatly reduce dispersion in anomalous samples, but
510 generally shifts ages to lower values that in some cases seem far too young based on
511 previous thermochronological results from this part of the TAM. Second, correction based
512 on the simple removal of ^{4}He released as spikes and at high temperatures implicitly relies
513 on the assumption that all these anomalous components are “extraneous” (i.e., these
514 components are not part of the syn- and post-closure radiogenic daughter production)
515 and therefore should be omitted for age calculation. However, such an assumption is
516 likely unfounded for reasons we now elaborate on.

517 **4.5 A conceptual ^{4}He transport model for apatite**

518 It would be ideal to have a framework that could reconcile the observed intra-sample
519 dispersion in AHe ages, anomalous outgassing components, and kinetic variations.
520 Consider an apatite that acquired a blend of crystal imperfections including both defects
521 and sinks immediately after its crystallization or perhaps later, during deformation; this
522 would almost certainly be the norm. As this apatite cooled but was still warmer than its
523 closure temperature for ^{4}He, during its random walk diffusing radiogenic ^{4}He could be
524 trapped in any larger crystal imperfections acting as sinks. The accumulation of this

trapped early radiogenic component would be extraneous with respect to normal expectations about cooling ages. This trapping would be controlled by the density of potentially many types of sinks of various sizes. In contrast, at low temperatures in nature where diffusion occurs extremely slowly, there would be little or no trapping in sinks of radiogenic production. Thus, natural samples would contain radiogenic ^{4}He in two different locations: “normal” lattice sites, and sinks, with the sinks filled only with atoms that had undergone significant numbers of diffusion jumps at higher temperatures. The amount of ^{4}He in sinks would be in proportion to the number of sinks present, the ability of ^{4}He to escape from sinks, and the thermal history, since slow cooling or isothermal thermal histories will permit extended intervals over which diffusing atoms could encounter a sink, in contrast to a quenched thermal history in which almost all radiogenic production occurred at low temperature.

When laboratory outgassing is then performed, all ^{4}He that has not encountered a sink would begin to be released through volume diffusion and this component would appear in the area under the first peak of the *df c*urve. However, atoms that are part of this “normal” diffusing component would also have a high probability of encountering sinks during laboratory heating. Thus, trapping could occur during two phases: for higher-temperature components (i.e., at temperatures above closure) in geologic times, and for all components during outgassing in the laboratory. Finally, at higher laboratory temperatures, any ^{4}He trapped in sinks, including ^{4}He that was trapped both in natural and in laboratory processes, would see a high probability of escaping to return to the volume-diffusion regime, and be manifested in the second high-temperature release peak

around ~800°C. In detail, given the nature of random walks in diffusion, atoms might become trapped and released multiple times, depending on the kinetics of trap escape.

Zeitler et al. (2017) pointed out that given the large number of diffusion jumps needed for an atom to escape from a crystal, the probability becomes very high that an atom will encounter a feature within the lattice. This agrees with our conclusion that gas-release spikes are sourced from imperfections located very near the grain surface and our observation that even very badly behaved grains show only a few such spikes. The number of sinks within a grain need not be very large or voluminous to significantly alter diffusion systematics within a grain.

In this model, age correction that removes all of the laboratory high-temperature gas-release would result in an underestimation of the amount of ^{4}He expected from closure theory and therefore yield an overcorrected age. The degree of overcorrection would be worst for a rapid-cooled sample in which almost all trapping happened in the laboratory, and least for a sample taken directly from the partial retention zone, for which a significant fraction of its ^{4}He found in sinks arrived there in nature.

What is challenging but interesting is that the ratio of low- to high-temperature gas release in the laboratory is a sample-specific property that will be controlled not only by the amount and type of traps, but also by the sample's thermal history. These factors will determine what proportion of the sample's ^{4}He content was geologically mobile and thus prone to trapping under natural conditions. Thus, the presence of a secondary CRH release peak is most directly an indication that sink-related crystal imperfections are

present in the sample. Whether a useful age correction can be developed under this model is unclear and will require further work. However, it is worth noting that for a given sample, all of the grains will have experienced the same thermal history, therefore the remaining dispersion in AHe ages after accounting for grain size and radiation damage via eU suggest that other types and / or density of defects are present. An interesting unanswered question is whether the presence of larger imperfections as revealed by CRH would stand as a proxy for the presence of finer-scale defects that might impede diffusion but not lead to trapping. This model also presents a new possibility in AHe thermochronology in that the pre- and syn- closure accumulation of extraneous ^{4}He and its laboratory release at high temperatures may offer the potential to recover additional constraints on thermal history (e.g., at earlier times at higher temperatures).

4.6 Kinetic variability beyond radiation-damage models

CRH results from apatites that pass CRH screening shed light on first-order kinetic variability of ^{4}He diffusion kinetics. Arrhenius plots from well-behaved grains show a significant range of intra-sample kinetic variability remains after grain size and eU effects are taken into account (**Fig. 8**). Additionally, while we observed some modest variations in the small amounts of Si and Ce present in TAM apatites (**Section 2.2.1**), these variations are not likely to lead to significant variations in the kinetics of fission-track annealing, nor does variation in the Cl and OH content of these fluorapatites (Barbarand et al., 2003). One might infer that this could apply to ^{4}He diffusion kinetics as well. The published results relating apatite composition to changes in ^{4}He diffusivity are mixed and likely complicated by the use of the FT annealing proxy Dpar. However, there is a direct correlation between apatite composition and track annealing. Djimbi et al. (2015)

591 discussed calculations showing that endmember fluorapatite and chlorapatites *should*
592 have somewhat different He diffusion kinetics, however the small variation in the TAM
593 apatites suggests that halogen composition is not likely to be a significant source of the
594 kinetic variations we observed.

595 This suggests that the defects that we observed are present in varying amounts (Section
596 2.2.2) and are altering the samples' diffusion kinetics – augmenting diffusivity changes
597 due to radiation damage. This is not a surprise given how past experimental and modeling
598 studies have shown that He diffusivity in apatite is influenced by fine-scale radiation
599 damage (Flowers et al., 2009; Gautheron et al., 2009; Shuster and Farley, 2009;), with
600 pristine lattices being associated with much more rapid diffusion. Note also that in data
601 presented by Flowers et al. (2009), while radiation damage is clearly a first-order control
602 on retentivity, considerable scatter remains that we would argue reflects the presence of
603 other defects, the impacts of which would matter particularly in settings involving slow
604 cooling or thermal stagnation, where greater single-grain age dispersion often appears
605 (e.g., Reiners and Farley 2001, Fitzgerald et al., 2006).

606 **4.7 Application of CRH screening to TAM exhumation**

607 Fitzgerald et al. (2006) documented that relatively slow cooling through the late
608 Cretaceous (~1 °C/m.y.) was followed by slightly more rapid cooling (< 3 °C/m.y.) as
609 constrained by the AFT age-elevation profile and inverse thermal-history modeling, but
610 as discussed earlier, their over-dispersed AHe single-grain ages were not able to further
611 constrain the cooling/exhumation history. A final question that remains is whether after
612 extensive analysis, we are able to place better constraints on the Eocene-Oligocene

613 cooling low-temperature history for the Cathedral Rocks profile. Our samples that passed
614 screening still show considerable age dispersion, and a critical question for us is whether
615 and how to assign thermochronologically meaningful weight to each AHe age.

616 We would argue that without assessment of individual-grain diffusion kinetics, one would
617 be uncertain about the thermal history constrained by a particular AHe age. In the case
618 of our samples, the ability of CRH analysis to screen apatites based on consistent criteria
619 – unimodal *df* curves – permits us to focus on a less dispersed subset of our data. Next,
620 note that a further subset of the screened data has ^{4}He diffusion kinetics similar to those
621 of Durango apatite, and all our other grains are considerably more retentive: just using
622 the offset in diffusivity seen across samples, some might be up to 25 to 30˚C more
623 retentive in closure temperature than Durango apatite, meaning that their retentivity (i.e.,
624 temperature sensitivity) begins to approach that of fission tracks in apatite.

625 If we simply focus on ages from CRH-screened grains having kinetics close to Durango,
626 we do obtain better temporal constraints and evidence for a faster-cooling episode in the
627 Cenozoic (**Fig. 9, filled diamond**). This new interpretation allows us to infer that more
628 rapid rock exhumation began at or by 35-40 Ma and is quite consistent with the thermal
629 history proposed for the Peak 1880 profile on the north side of the Ferrar Glacier (**Fig. 1;**
630 **Fig. 9**) where AHe dates are less dispersed. Such increase in cooling/exhumation rate at
631 ca. 35 Ma is also a cooling/exhumation signal seen at a number of locations along the
632 TAM. This signal has been interpreted as tectonic, either due to dextral-transtension
633 (Olivetti et al., 2013, 2018) or rifting and escarpment retreat further south along the
634 Transantarctic Mountain front (Miller et al. 2010). Alternatively, the timing of this enhanced

exhumation in the Late-Eocene-early Oligocene has been attributed to enhanced erosion due to the onset of glaciation in Antarctica at ~35 Ma (e.g., He et al., 2019; Thomson et al., 2019).

5. Conclusions

Assessment of outgassing components and evaluation of age corrections suggests that ^{4}He transportation in apatite might be controlled by more complex models than are currently being used. We argue that CRH analysis can be used to empirically screen apatites for ^{4}He components trapped in sinks, and additionally permit assessment as to whether diffusion is behaving as expected from volume diffusion and radiation-damage models. In this regard, we found the youngest cluster of screened AHe ages from the Cathedral Rocks in the Transantarctic Mountains, which were characterized by unimodal ^{4}He outgassing behavior and Durango-like kinetics, suggest rapid rock exhumation at *ca.* 35 Ma, which is consistent with regional initiation of glaciation at the end of the Eocene (ref. Ivany et al., 2006).

Our findings underscore the important message that simple volume diffusion and current radiation-damage models may be insufficient to extract rock thermal histories for some apatite populations. CRH screening analysis can characterize ^{4}He diffusion systematics in as little as 30 minutes per aliquot, making it suitable for routine dating. Having information such as this in hand before attempting age interpretations and modeling seems to us far more preferable than relying on statistical manipulation or analysis of numerous grains to address age dispersion after the fact. We recommend more

widespread deployment of CRH or $^{4}He/^{3}He$ for AHe dating, especially for sample suites that show significant age dispersion.

Acknowledgements

Both this work and part of HG's graduate study were supported by the National Science Foundation [grant EAR-1726350 to AKF, PKZ, and BDI]; PGF acknowledges support from the National Science Foundation [grants OPP-0002824 and OPP-9615294] for the original (U-Th)/He work along the TAM. The rock samples were originally collected as part of Antarctic fieldwork through the Antarctic Research Centre of Victoria University of Wellington with samples originally processed by Fitzgerald at the University of Melbourne, Australia. We thank Peter Reiners, Uttam Chowdhury, and the Arizona Radiogenic Dating Laboratory for U-Th-Sm-Ca measurements. Quantitative analyses were performed on a JEOL JXA-8530FPlus electron microprobe at the University of Minnesota. Funding for electron microprobe facility used in this research was provided by NSF under award number EAR-1625422. Most graphs created using Generic Mapping Tools (GMT) v. 6.0 (Wessel et al., 2019).

Research Data

Research Data associated with this article can be accessed via Harvard Dataverse at https://doi.org/10.7910/DVN/FWAZHT

References

Allibone A. H., Cox S. C., Graham I. J., Smellie R. W., Johnstone R. D., Ellery S. G. and Palmer K. (1993) Granitoids of the Dry Valleys area, southern Victoria Land, Antarctica: plutons, field relationships, and isotopic dating. *N. Z. J. Geol. Geophys.* **36,** 281-297.

Ault A. K., Gautheron C. and King G. E. (2019) Innovations in (U–Th)/He, fission track, and trapped charge thermochronometry with applications to earthquakes, weathering, surface-mantle connections, and the growth and decay of mountains. *Tectonics* **38,** 3705-3739.

Barbarand J., Carter A., Wood I. and Hurford T. (2003) Compositional and structural control of fission-track annealing in apatite. *Chem. Geol.* **198,** 107-137.

Baxter E. F. (2003) Quantification of the factors controlling the presence of excess 40Ar or 4He. *Earth Planet. Sci. Lett.* **216,** 619-634.

Beucher R., Brown R. W., Roper S., Stuart F. and Persano C. (2013) Natural age dispersion arising from the analysis of broken crystals: Part II. Practical application to apatite (U–Th)/He thermochronometry. *Geochim. Cosmochim. Acta* **120,** 395-416.

Brown R. W., Beucher R., Roper S., Persano C., Stuart F. and Fitzgerald P. (2013) Natural age dispersion arising from the analysis of broken crystals. Part I: Theoretical basis and implications for the apatite (U–Th)/He thermochronometer. *Geochim. Cosmochim. Acta* **122,** 478-497.

Cooperdock E. H., Ketcham R. A. and Stockli D. F. (2019) Resolving the effects of 2-D versus 3-D grain measurements on apatite (U–Th)/He age data and reproducibility. *Geochronology* **1,** 17-41.

Dalziel I. W. (1992) Antarctica; a tale of two supercontinents? *Annu. Rev. Earth Planet. Sci.* **20,** 501-526.

Djimbi D. M., Gautheron C., Roques J., Tassan-Got L., Gerin C. and Simoni E. (2015) Impact of apatite chemical composition on (U-Th)/He thermochronometry: An atomistic point of view. *Geochim. Cosmochim. Acta* **167,** 162-176.

Domingos R., Tremblay M. M., Shuster D. L. and Militzer B. (2020) Simulations and Experiments Reveal Effect of Nanopores on Helium Diffusion in Quartz. *ACS Earth Space Chem.* **4,** 1906-1912.

Farley K. A. (2000) Helium diffusion from apatite: General behavior as illustrated by Durango fluorapatite. *Journal of Geophysical Research: Solid Earth* **105,** 2903-2914.

709 Farley K. A., Wolf R. A. and Silver L. T. (1996) The effects of long alpha-stopping
710 distances on (U-Th)/He ages. *Geochim. Cosmochim. Acta* **60,** 4223-4229.

711 Farley K. A. (2002) (U-Th)/He dating: Techniques, calibrations, and
712 applications. *Reviews in Mineralogy and Geochemistry* **47,** 819-844.

713 Fitzgerald P. G., Baldwin S. L., Webb L. E. and O'Sullivan P. B. (2006) Interpretation of
714 (U–Th)/He single grain ages from slowly cooled crustal terranes: a case study from
715 the Transantarctic Mountains of southern Victoria Land. *Chem. Geol.* **225,** 91-120.

716 Florindo F., Wilson G. S., Roberts A. P., Sagnotti L. and Verosub K. L. (2001)
717 Magnetostratigraphy of late Eocene-early Oligocene strata from the CRP-3 core,
718 Victoria Land Basin, Antarctica. *Terra Antartica* **8,** 599-614.

719 Flowers R. M. and Farley K. A. (2012) Apatite $^{4}He/^{3}He$ and (U-Th)/He evidence for an
720 ancient Grand Canyon. *Science* **338,** 1616-1619.

721 Flowers R. M. and Kelley S. A. (2011) Interpreting data dispersion and “inverted” dates
722 in apatite (U–Th)/He and fission-track datasets: an example from the US
723 midcontinent. *Geochim. Cosmochim. Acta* **75,** 5169-5186.

724 Flowers R. M., Ketcham R. A., Shuster D. L. and Farley K. A. (2009) Apatite (U–Th)/He
725 thermochronometry using a radiation damage accumulation and annealing
726 model. *Geochim. Cosmochim. Acta* **73,** 2347-2365.

727 Galeotti S., DeConto R., Naish T., Stocchi P., Florindo F., Pagani M., Barrett P., Bohaty
728 S. M., Lanci L. and Pollard D. (2016) Antarctic Ice Sheet variability across the
729 Eocene-Oligocene boundary climate transition. *Science* **352,** 76-80.

730 Gautheron C., Tassan-Got L., Barbarand J. and Pagel M. (2009) Effect of alpha-
731 damage annealing on apatite (U-Th)/He thermochronology. *Chem. Geol.* **266,** 157-
732 170.

733 Gerin C., Gautheron C., Oliviero E., Bachelet C., Djimbi D. M., Seydoux-Guillaume A.,
734 Tassan-Got L., Sarda P., Roques J. and Garrido F. (2017) Influence of vacancy
735 damage on He diffusion in apatite, investigated at atomic to mineralogical
736 scales. *Geochim. Cosmochim. Acta* **197,** 87-103.

737 Goodge J. W. (2020) Geological and tectonic evolution of the Transantarctic Mountains,
738 from ancient craton to recent enigma. *Gondwana Research* **80,** 50-122.

739 Green P. and Duddy I. (2018) Apatite (U-Th-Sm)/He thermochronology on the wrong
740 side of the tracks. *Chem. Geol.* **488,** 21-33.

741 Gunn B. M. and Warren G. (1962) *Geology of Victoria Land between the Mawson and*
742 *Mulock Glaciers, Antarctica.* Trans-Antarctic Expedition Committee,

743 He J., Thomson S. N. and Reiners P. W. (2019) Apatite (U-Th)/He thermochronometric
744 data show rapid late Eocene incision in the central Transantarctic Mountains. *AGU*
745 *Fall Meeting,* C53B-1340.

Idleman B. D., Zeitler P. K. and McDannell K. T. (2018) Characterization of helium release from apatite by continuous ramped heating. *Chem. Geol.* **476,** 223-232.

Ivany L. C., Van Simaeys S., Domack E. W. and Samson S. D. (2006) Evidence for an earliest Oligocene ice sheet on the Antarctic Peninsula. *Geology* **34,** 377-380.

Karato S. (2008) *Deformation of Earth Materials: An Introduction to the Rheology of Solid Earth.* Cambridge University Press, Cambridge.

Ketcham R. A., Carter A., Donelick R. A., Barbarand J. and Hurford A. J. (2007) Improved modeling of fission-track annealing in apatite. *Am. Mineral.* **92,** 799-810.

Ketcham R. A., Gautheron C. and Tassan-Got L. (2011) Accounting for long alpha-particle stopping distances in (U-Th-Sm)/He geochronology: refinement of the baseline case. *Geochim. Cosmochim. Acta* **75,** 7779-7791.

Krogh T. E. (1982) Improved accuracy of U-Pb zircon ages by the creation of more concordant systems using an air abrasion technique. *Geochim. Cosmochim. Acta* **46,** 637-649.

Lippolt H. J., Leitz M., Wernicke R. S. and Hagedorn B. (1994) (Uranium thorium)/helium dating of apatite: experience with samples from different geochemical environments. *Chem. Geol.* **112,** 179-191.

Long S. P., Thomson S. N., Reiners P. W. and Di Fiori R. V. (2015) Synorogenic extension localized by upper-crustal thickening: An example from the Late Cretaceous Nevadaplano. *Geology* **43,** 351-354.

McDannell K. T., Zeitler P. K., Janes D. G., Idleman B. D. and Fayon A. K. (2018) Screening apatites for (U-Th)/He thermochronometry via continuous ramped heating: He age components and implications for age dispersion. *Geochim. Cosmochim. Acta* **223,** 90-106.

McDowell F. W., McIntosh W. C. and Farley K. A. (2005) A precise ^{40}Ar–^{39}Ar reference age for the Durango apatite (U–Th)/He and fission-track dating standard. *Chem. Geol.* **214,** 249-263.

Meesters A. and Dunai T. J. (2002) Solving the production–diffusion equation for finite diffusion domains of various shapes: Part II. Application to cases with α-ejection and nonhomogeneous distribution of the source. *Chem. Geol.* **186,** 57-73.

Murray K. E., Orme D. A. and Reiners P. W. (2014) Effects of U-Th-rich grain boundary phases on apatite helium ages. *Chem. Geol.***390,** 135-151.

Peyton S. L., Reiners P. W., Carrapa B. and DeCelles P. G. (2012) Low-temperature thermochronology of the northern Rocky Mountains, western USA. *Am. J. Sci.* **312,** 145-212.

Piccoli P. M. and Candela P. A. (2002) Apatite in igneous systems. *Reviews in Mineralogy and Geochemistry* **48,** 255-292.

Reiners P. W., Ehlers T. A., Mitchell S. G. and Montgomery D. R. (2003) Coupled spatial variations in precipitation and long-term erosion rates across the Washington Cascades. *Nature* **426,** 645-647.

Reiners P. W., Ehlers T. A. and Zeitler P. K. (2005) Past, present, and future of thermochronology. *Reviews in Mineralogy and Geochemistry* **58,** 1-18.

Reiners P. W. and Farley K. A. (2001) Influence of crystal size on apatite (U–Th)/He thermochronology: an example from the Bighorn Mountains, Wyoming. *Earth Planet. Sci. Lett.* **188,** 413-420.

Shuster D. L., Flowers R. M. and Farley K. A. (2006) The influence of natural radiation damage on helium diffusion kinetics in apatite. *Earth Planet. Sci. Lett.* **249,** 148-161.

Shuster D. L. and Farley K. A. (2009) The influence of artificial radiation damage and thermal annealing on helium diffusion kinetics in apatite. *Geochim. Cosmochim. Acta* **73,** 183-196.

Smellie J. L. (2001) History of Oligocene erosion, uplift and unroofing of the Transantarctic Mountains deduced from sandstone detrital modes in CRP-3 drillcore, Victoria Land Basin, Antarctica. *Terra Antartica* **8,** 481-490.

Spiegel C., Kohn B., Belton D., Berner Z. and Gleadow A. (2009) Apatite (U–Th–Sm)/He thermochronology of rapidly cooled samples: the effect of He implantation. *Earth Planet. Sci. Lett.* **285,** 105-114.

Thomson S. N., Reiners P. W., He J., Hemming S. R. and Licht K. (2019) New constraints on the pre-glacial and glacial uplift and incision history of the central Transantarctic Mountains using multiple low-temperature thermochronometers. *AGU Fall Meeting***,** C14B-04.

Toraman E., Teyssier C., Whitney D. L., Fayon A. K., Thomson S. N. and Reiners P. W. (2014) Low-temperature thermochronologic record of Eocene migmatite dome emplacement and late Cenozoic landscape development, Shuswap core complex, British Columbia. *Tectonics* **33,** 1616-1635.

Watson E. B. and Cherniak D. J. (2003) Lattice diffusion of Ar in quartz, with constraints on Ar solubility and evidence of nanopores. *Geochim. Cosmochim. Acta* **67,** 2043-2062.

Wessel P., Luis J. F., Uieda L., Scharroo R., Wobbe F., Smith W. and Tian D. (2019) The generic mapping tools version 6. *Geochem. Geophys. Geosyst.* **20,** 5556-5564.

Willett C. D., Fox M. and Shuster D. L. (2017) A helium-based model for the effects of radiation damage annealing on helium diffusion kinetics in apatite. *Earth Planet. Sci. Lett.* **477,** 195-204.

Wilson G. S., Roberts A. P., Verosub K. L., Florindo F. and Sagnotti L. (1998) Magnetobiostratigraphic chronology of the Eocene—Oligocene transition in the

CIROS-1 core, Victoria Land margin, Antarctica: Implications for Antarctic glacial history. *Geological Society of America Bulletin* **110,** 35-47.

Wolf R. A., Farley K. A. and Silver L. T. (1996) Helium diffusion and low-temperature thermochronometry of apatite. *Geochim. Cosmochim. Acta* **60,** 4231-4240.

Zeitler P. K., Herczeg A. L., McDougall I. and Honda M. (1987) U-Th-He dating of apatite: A potential thermochronometer. *Geochim. Cosmochim. Acta* **51,** 2865-2868.

Zeitler, P., Brown R. and Hackspacher P. (2017), Better tools for tracing the thermal history of rocks. *Eos **98**,* doi:10.1029/2017EO073479.

Zeitler P. K., Enkelmann E., Thomas J. B., Watson E. B., Ancuta L. D. and Idleman B. D. (2017) Solubility and trapping of helium in apatite. *Geochim. Cosmochim. Acta* **209,** 1-8.

Figure Captions

Figure 1. (A) Simplified map of southern Victoria Land showing location of the two vertical sampling profiles from Peak 1880 and Cathedral Rocks. Filled areas are ice free. TAM: Transantarctic Mountains. (B and C) Composite AFT and AHe plots summarizing the preferred cooling/exhumation path (dashed line) for the two vertical profiles but with AHe data moved down in elevation relative to the AFT data based on the difference in closure temperatures (30 – 35 °C) divided by the estimated paleogeothermal gradient (20 – 35 °C/km). Modified from Fitzgerald et al. (2006). For the AHe data, Fitzgerald et al. (2006) judged that younger AHe ages (between the minimum age and a weighted mean) were more likely to constrain a "true" thermal history, perhaps an early precursor to using screened CRH-screened ages (as shown in this study, section 4.7). Less dispersion in the Peak 1880 AHe data allowed constraints to be placed on Late Eocene cooling, whereas much greater dispersion in AHe data from Cathedral Rocks precluded such constraints.

Figure 3. Incremental ^{4}He release (*df*) curves (A), and CRH-derived Arrhenius relationships (B) of Durango apatites under a 30 ˚C/min heating ramp rate. Gray curves and circles depict result from Durango shards; blue curves and triangles show result from Durango balls. Red dashed line marks diffusion kinetics of ^{4}He in Durango apatite acquired by Farley (2000) via step-heating, adjusted to a radius of 80 μm. (C) Arrhenius plot of the same analyses adjusted to a common spherical-equivalent radius of a = 80 μm in order to assess precision in the kinetics obtained by CRH, an indirect verification of temperature control. (D) shows the temperature uncertainties at two points for CRH analysis of Durango balls.

Figure 4. Single-grain AHe ages (upper plot) and RDAAM-normalized relative ages (lower plot). Ages from each sample are presented in individual panels. Each plot includes measured single-grain total-gas age, screened age, and CRH-corrected age, accompanied by their kernel density estimations (KDEs). For better visualization ages older than 100 Ma were omitted; Table A1 shows information for all ages.

Figure 5. Cathedral Rocks AHe and AFT age-elevation plots summarizing results and interpretations from this study and from Fitzgerald et al. (2006). Light blue circles and curves show single-grain total-gas AHe ages (this study) and their KDE, respectively; dark blue circles and shaded curves show single-grain screened AHe ages (this study) and their KDE; pink shaded curves show KDE of single-grain CRH-corrected ages; red circles show AHe weighed mean ages (Fitzgerald et al,, 2006); orange triangles show AFT central ages (Fitzgerald et al., 2006); red dashed line shows best-fit trend to the weighted mean AHe ages from Fitzgerald et al. (2006).

Figure 6. *df* curves measured using a 30 ˚C/min ramped heating schedule. Results from each sample are presented in individual subpanels. (A) Results from grains that passed CRH screening. (B) Results from grains that failed screenin*g*. (C) Results from all grains, color-coded into three groups: blue, grains whose AHe ages are not older than the oldest screened age in that sample; red, grains whose AHe ages are older than the fission-track central ages measured by Fitzgerald et al. (2006); orange, grains whose ages fall between the other two groups.

Figure 7. (A) Relationships between single-grain AHe age and grain size (total compilation shown in panel C). (B) Relationships between single-grain AHe age and equivalent uranium (eU) (total compilation shown in panel D). Sizes are calculated as F_T -equivalent spherical radius. To be consistent with prior publications eU is calculated as U + 0.235*Th; Cooperdock et al (2019) provide a more accurate update). Filled circles show grains that passed CRH screening.

Figure 8. CRH-derived Arrhenius relationships of apatite grains that passed CRH screening, showing relationship between AHe ages and apparent ^{4}He diffusivity. (A) Observed kinetics color-coded by observed age. (B) Kinetics adjusted to 80 μm radius, color-coded by observed age. (C) Kinetics adjusted to 80 μm radius, color-coded by RDAAM-normalized relative age. Dashed green line show the kinetics of ^{4}He diffusion in Durango apatites measured by Farley (2000). Vertical dotted line provides visual reference to aid comparison of diffusivity variations at 10000/K = 15 (~393.5 ˚C).

Figure 9. Composite AFT and AHe plot (constructed as Figure 1C) summarizing our updated cooling/exhumation path for the Cathedral Rocks locality. Preferred path for Peak 1880 is from Fitzgerald et al. (2006).

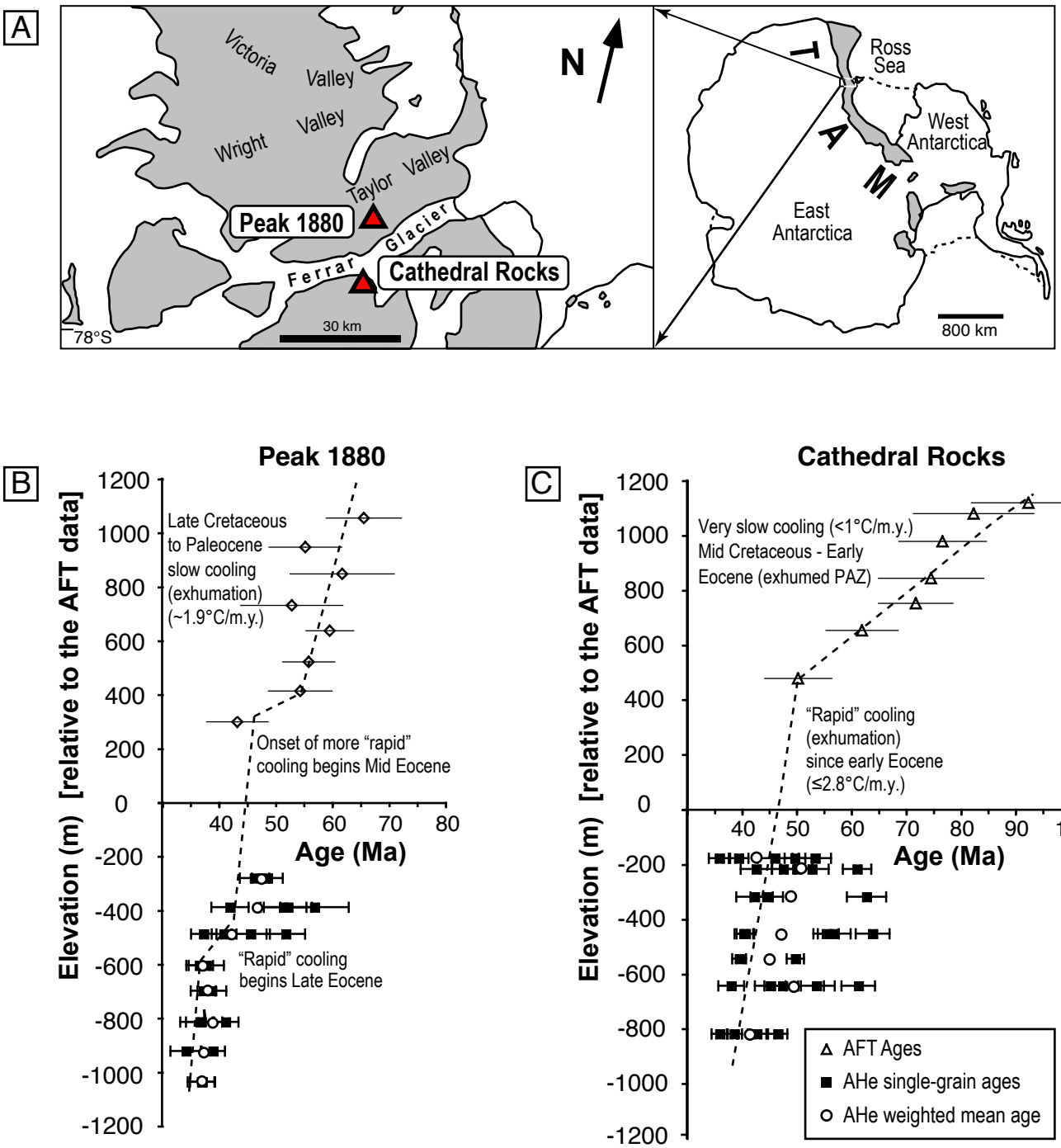

Figure. 1

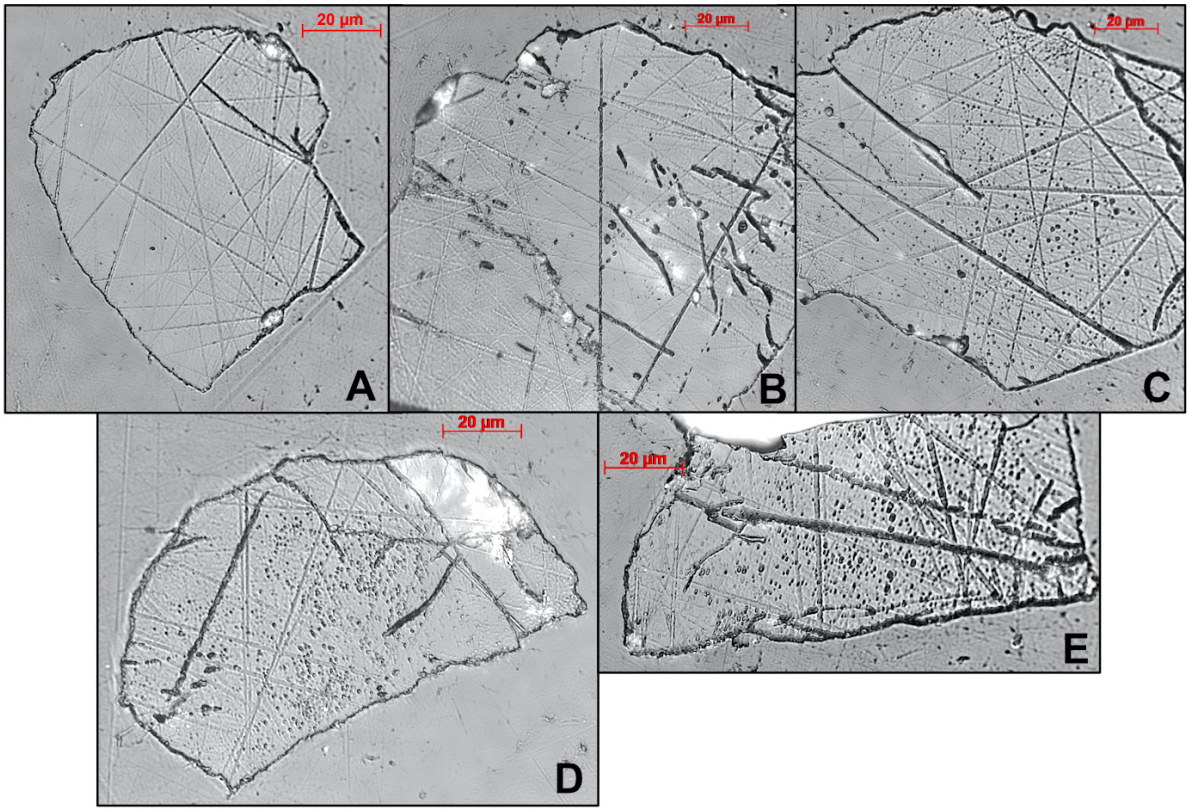

Figure 2

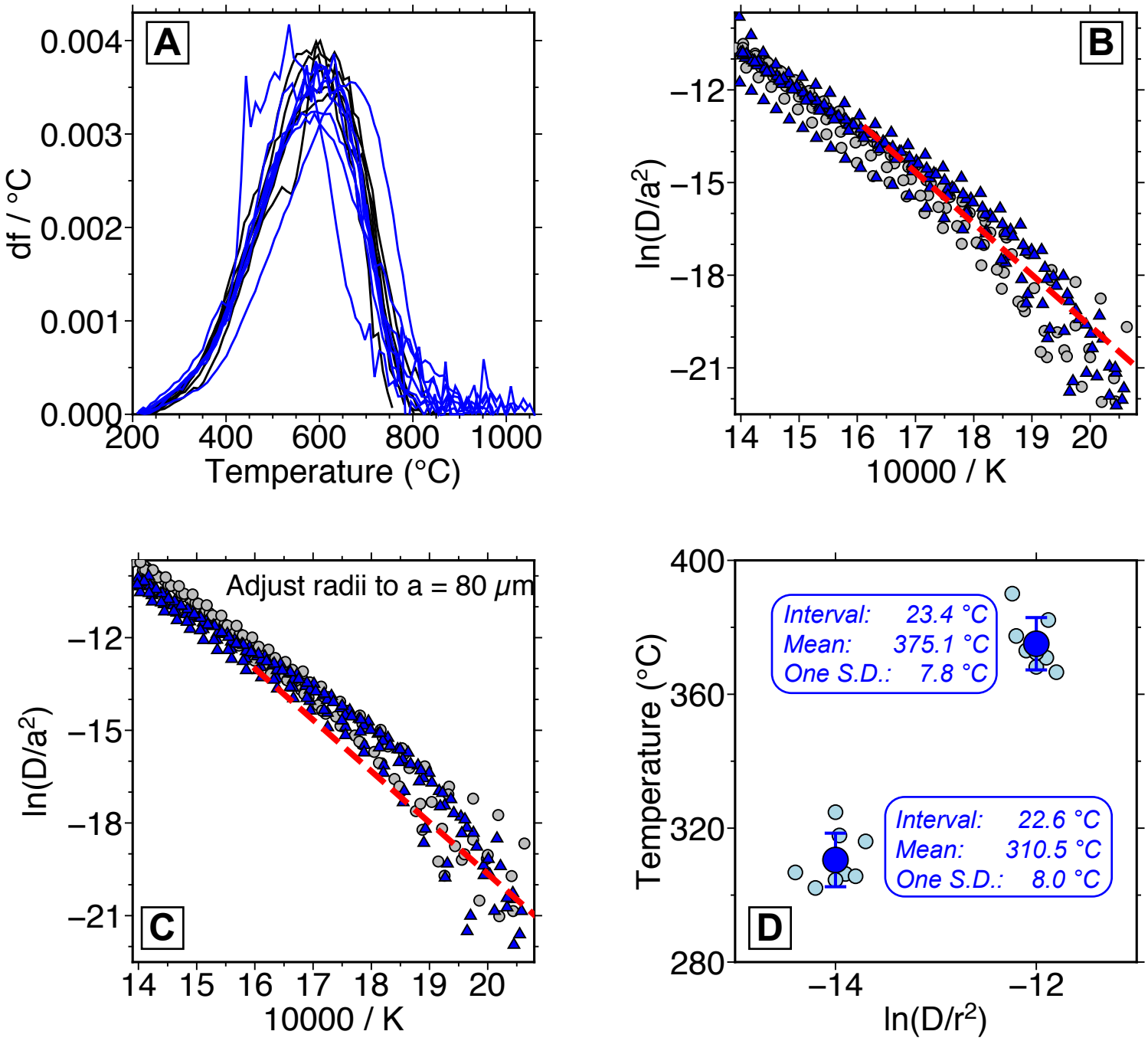

Figure 3

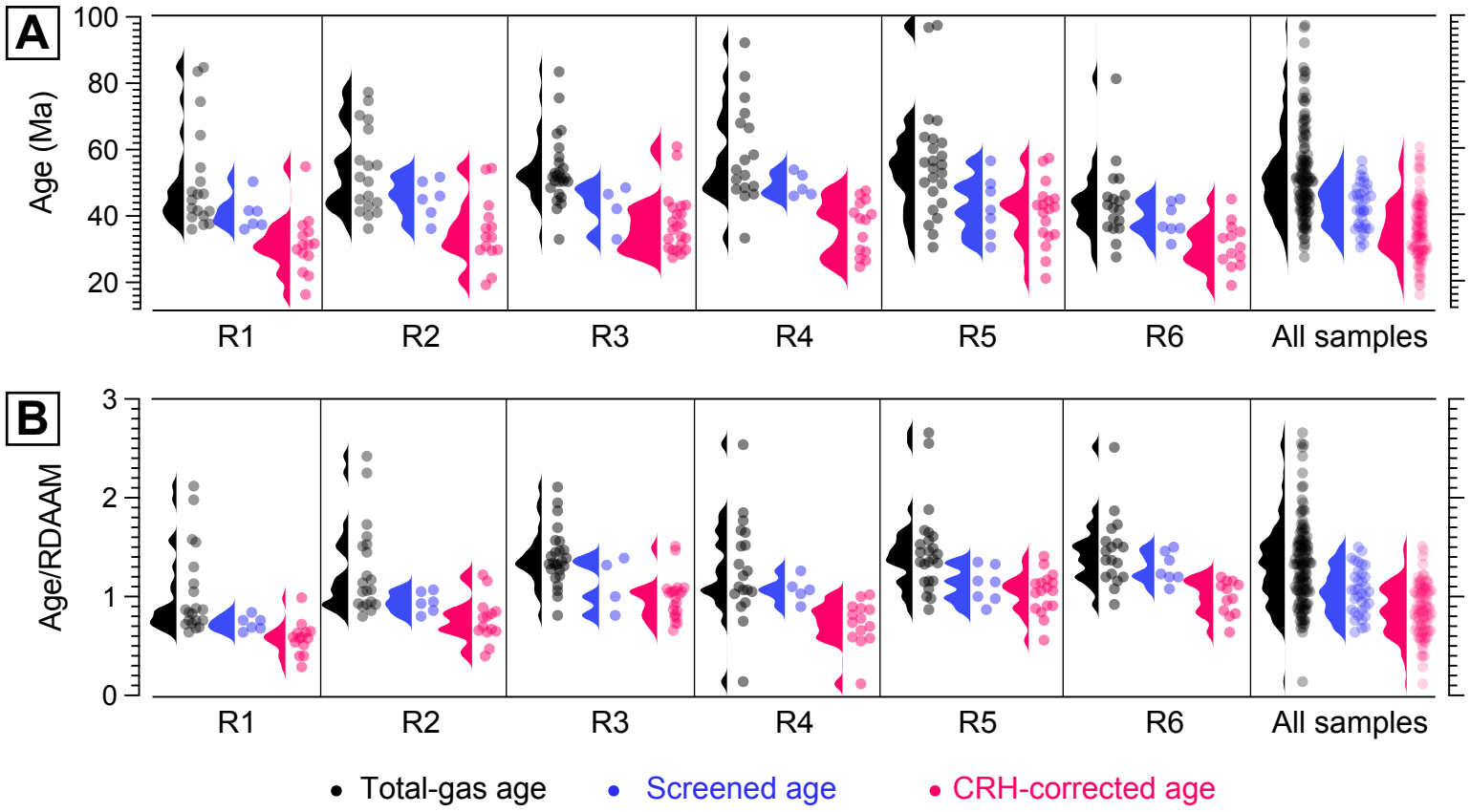

Figure 4

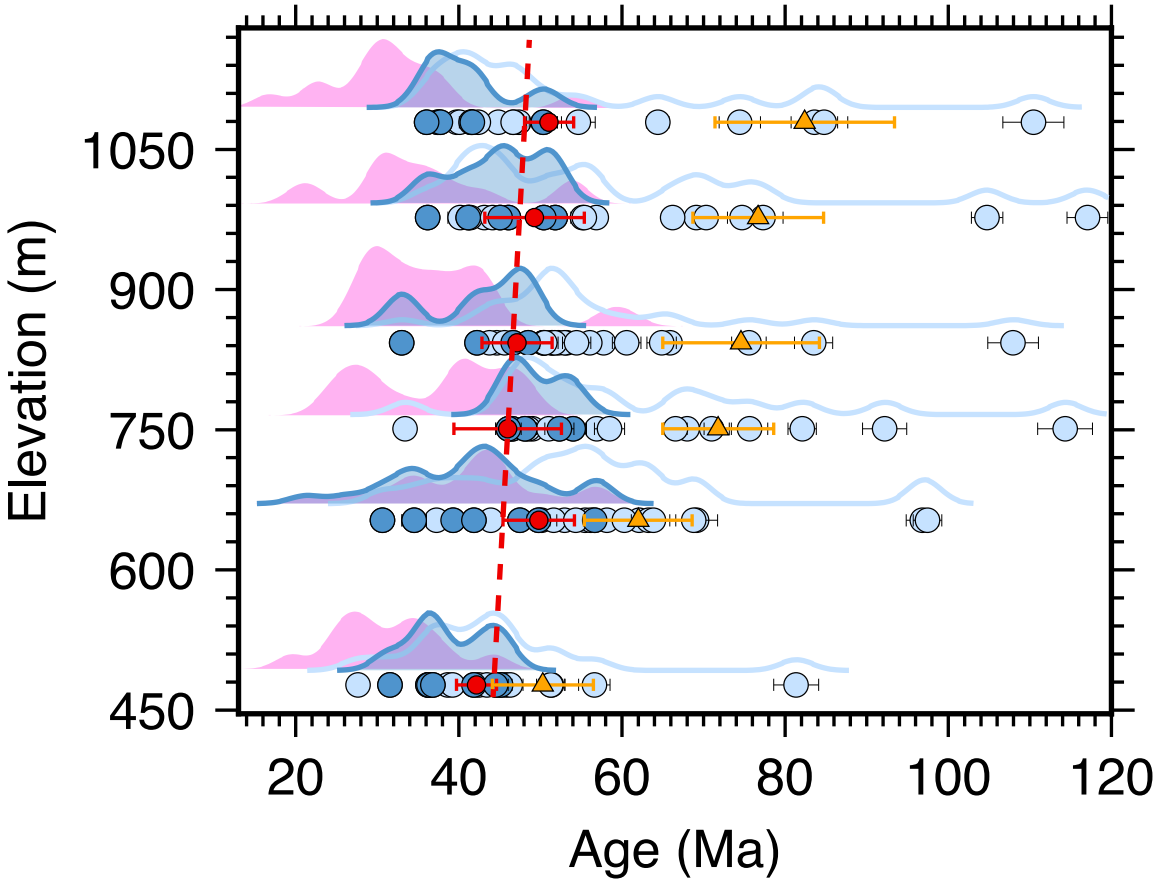

Figure 5

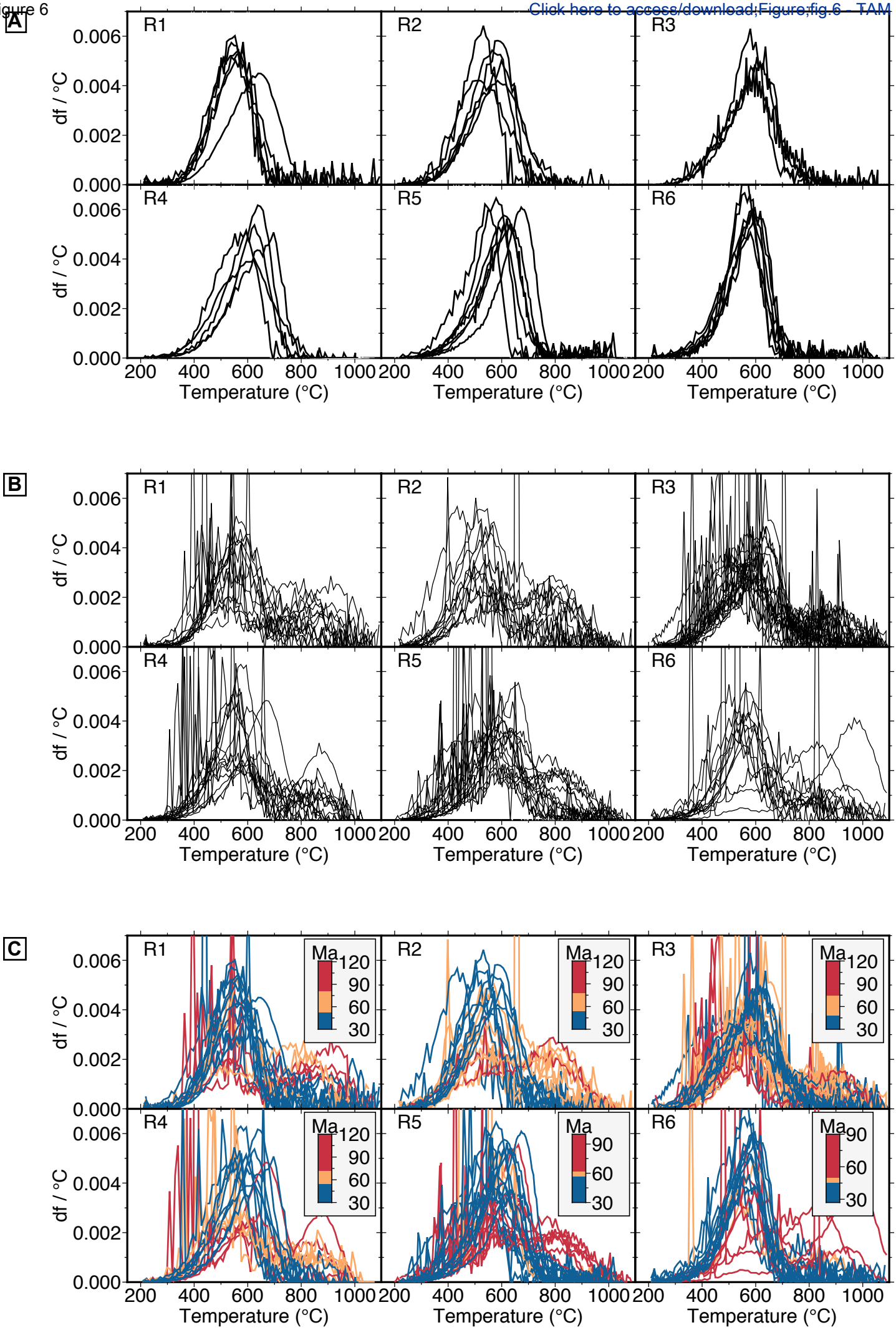

Figure 6

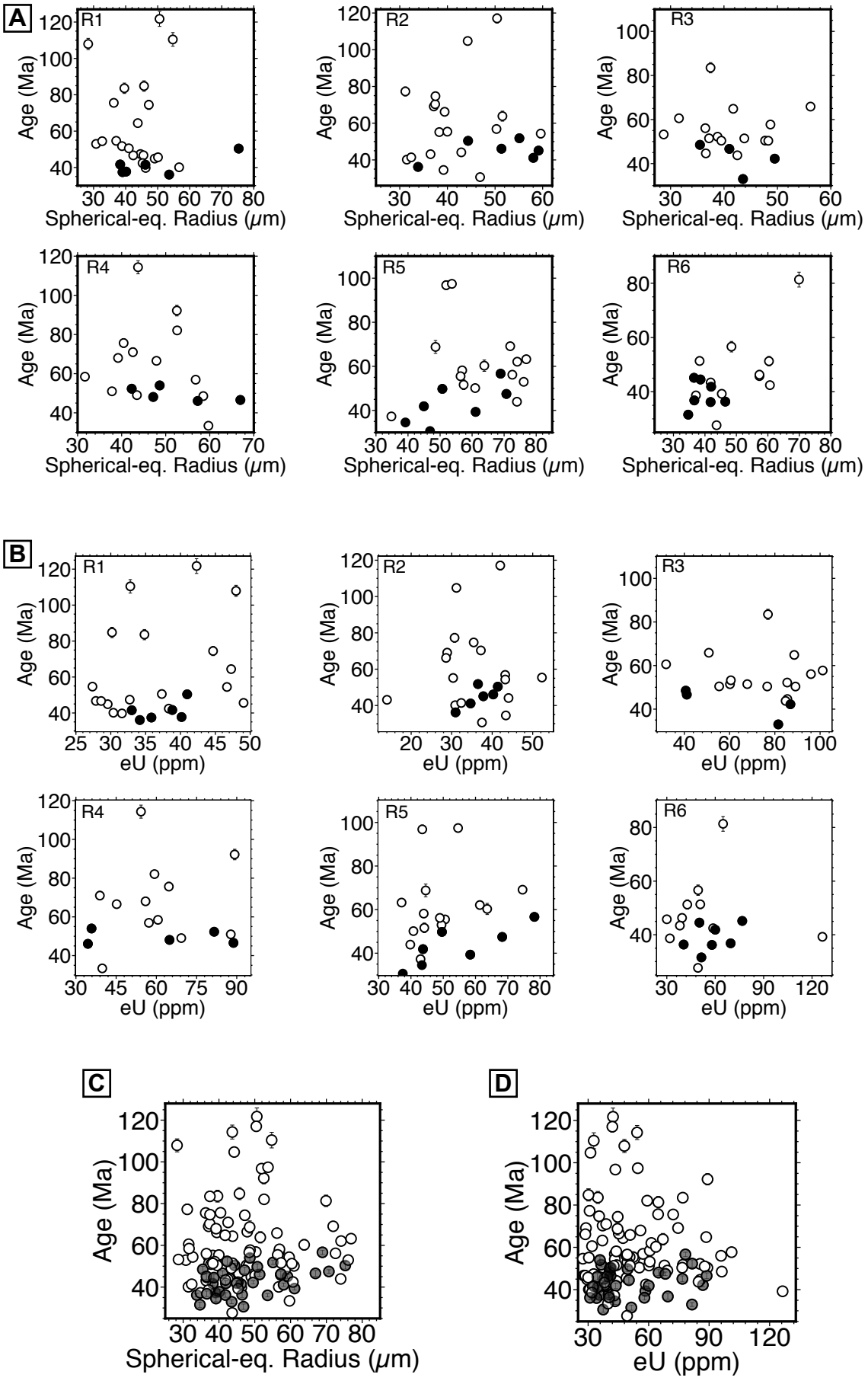

Figure 7

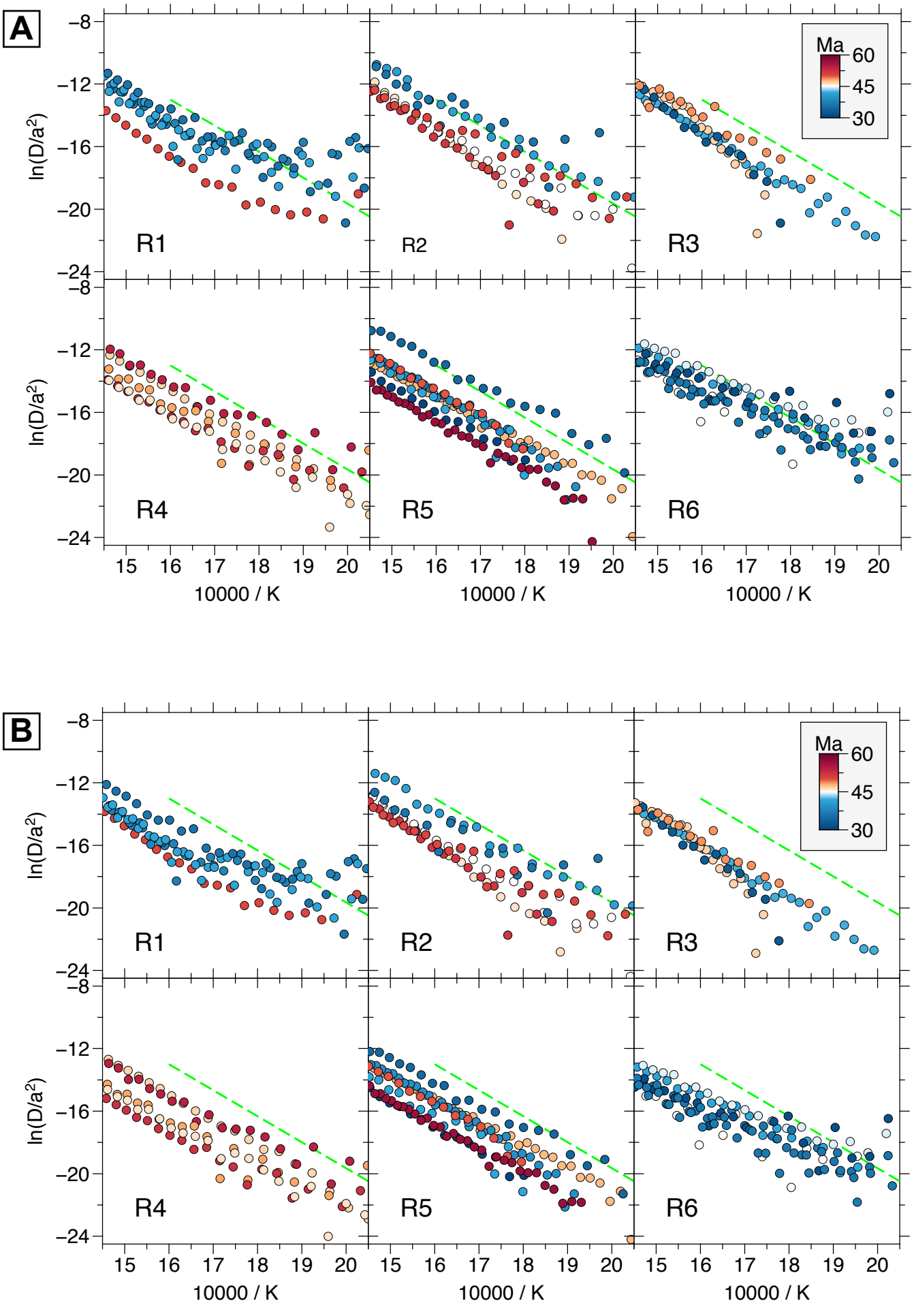

Figure 8

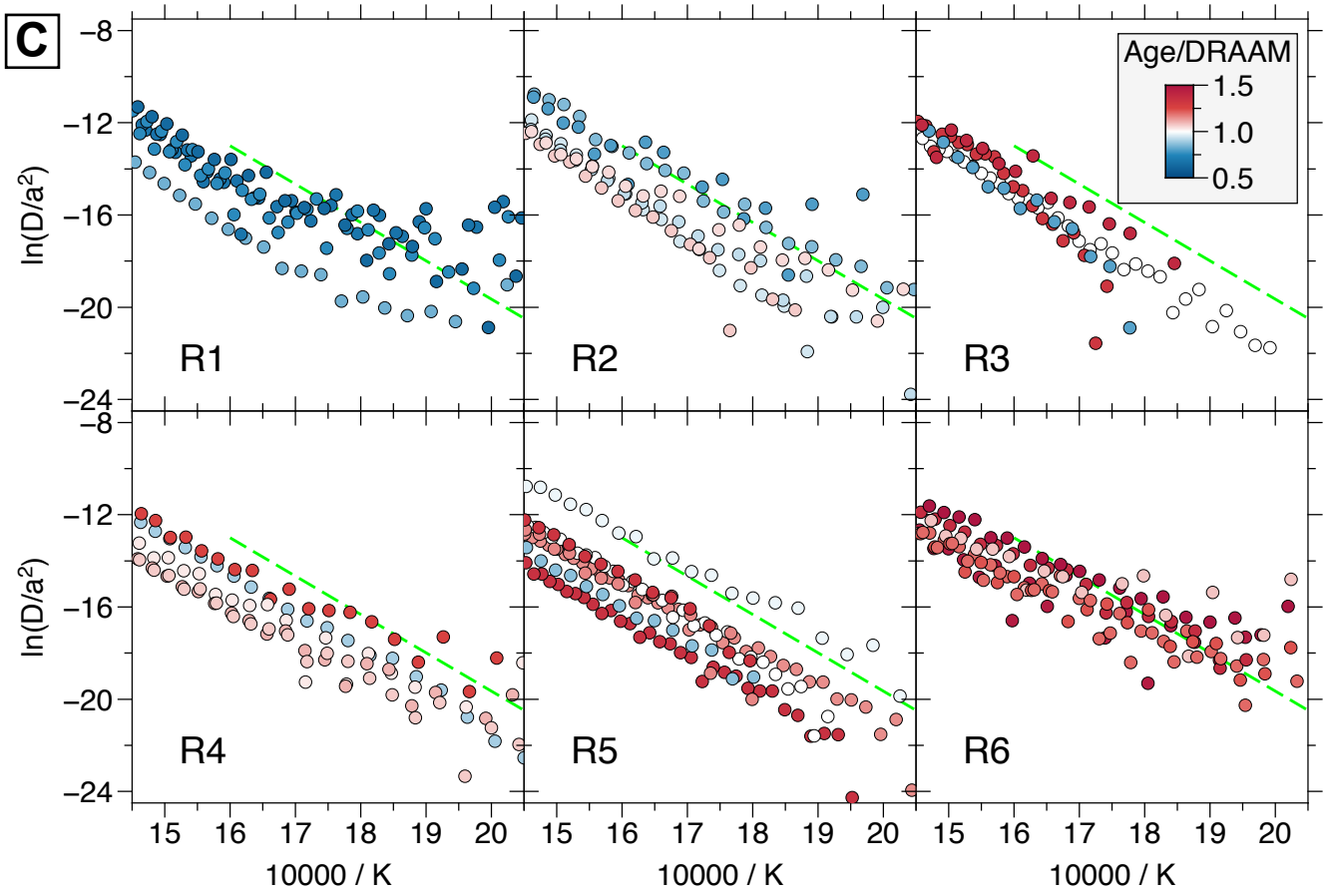

Figure 8 - continued

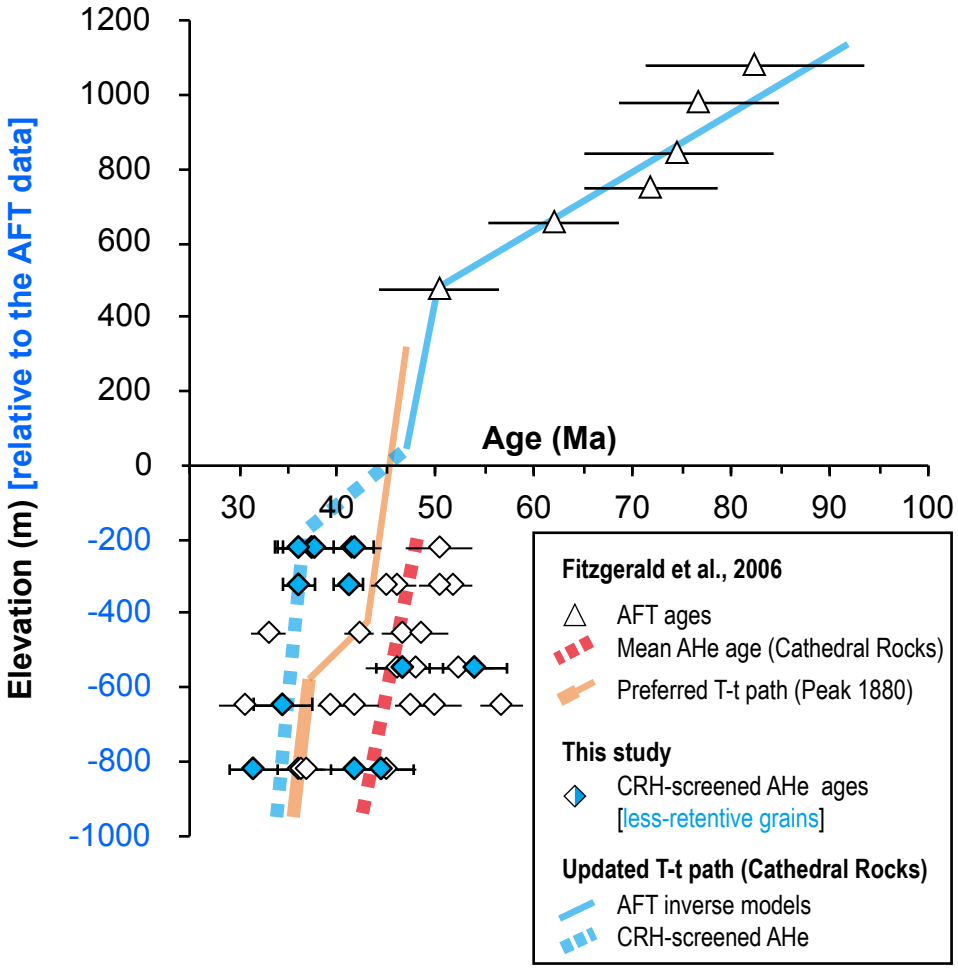

Figure 9

Appendix A

Click here to access/download

Appendix

Appendix_A.pdf